1526–1537 *Nucleic Acids Research, 2011, Vol. 39, No. 4* *Published online 23 October 2010*
doi:10.1093/nar/gkq931

The Bowen–Conradi syndrome protein Nep1 (Emg1) has a dual role in eukaryotic ribosome biogenesis, as an essential assembly factor and in the methylation of Ψ1191 in yeast 18S rRNA

Britta Meyer[1,2], Jan Philip Wurm[2,3], Peter Kötter[1,2], Matthias S. Leisegang[1,2], Valeska Schilling[1,2], Markus Buchhaupt[1,2], Martin Held[1,4], Ute Bahr[1,4], Michael Karas[1,4], Alexander Heckel[1,4], Markus T. Bohnsack[1,2], Jens Wöhnert[2,3] and Karl-Dieter Entian[1,2,*]

[1]Cluster of Excellence Frankfurt: Macromolecular Complexes, [2]Institute for Molecular Biosciences, [3]Center of Biomolecular Magnetic Resonance (BMRZ) and [4]Institute for Pharmaceutical Chemistry, Johann-Wolfgang Goethe University, Max-von-Laue Str. 9, D-60438 Frankfurt/M., Germany

Received March 18, 2010; Revised September 10, 2010; Accepted September 28, 2010

ABSTRACT

The Nep1 (Emg1) SPOUT-class methyltransferase is an essential ribosome assembly factor and the human Bowen–Conradi syndrome (BCS) is caused by a specific Nep1^{D86G} mutation. We recently showed *in vitro* that *Methanocaldococcus jannaschii* Nep1 is a sequence-specific pseudouridine-N1-methyltransferase. Here, we show that in yeast the *in vivo* target site for Nep1-catalyzed methylation is located within loop 35 of the 18S rRNA that contains the unique hypermodification of U1191 to 1-methyl-3-(3-amino-3-carboxypropyl)-pseudouridine (m1acp3Ψ). Specific ^{14}C-methionine labelling of 18S rRNA in yeast mutants showed that Nep1 is not required for acp-modification but suggested a function in Ψ1191 methylation. ESI MS analysis of acp-modified Ψ-nucleosides in a *Δnep1*-mutant showed that Nep1 catalyzes the Ψ1191 methylation *in vivo*. Remarkably, the restored growth of a *nep1-1^{ts}* mutant upon addition of *S*-adenosylmethionine was even observed after preventing U1191 methylation in a *Δsnr35* mutant. This strongly suggests a dual Nep1 function, as Ψ1191-methyltransferase and ribosome assembly factor. Interestingly, the Nep1 methyltransferase activity is not affected upon introduction of the BCS mutation. Instead, the mutated protein shows enhanced dimerization propensity and increased affinity for its RNA-target *in vitro*. Furthermore, the BCS mutation prevents nucleolar accumulation of Nep1, which could be the reason for reduced growth in yeast and the Bowen-Conradi syndrome.

INTRODUCTION

Eukaryotic ribosome biogenesis is highly regulated and much more complex than the corresponding pathway in prokaryotes. A large number of proteins and small nucleolar RNAs (snoRNAs) are involved in addition to the four rRNAs and ~80 core proteins of eukaryotic ribosomes. These non-ribosomal proteins and snoRNAs fulfil major functions in either rRNA modification or ribosome assembly. In conjunction with rRNA processing, ribosomal proteins and non-ribosomal factors assemble into pre-ribosomal particles in which further maturation steps take place (1,2). In fast-growing yeast cells, up to 2000 ribosomes are synthesized per minute and ~10% of the genomic information is needed for the biosynthesis of a ribosome (3). This includes more than 180 *trans*-acting proteins (e.g. nucleases, RNA-helicases and RNA-modifying enzymes), and ~75 small nucleolar RNAs (snoRNAs) (4,5). Numerous *trans*-acting proteins have orthologous functions in many eukaryotes, which allow the use of model organisms to understand their physiological function. In case of proteins involved in eukaryotic ribosome biogenesis, most of our knowledge was obtained from studies with baker's yeast (*Saccharomyces cerevisiae*) (6).

Most of the ribosome assembly steps take place in the nucleolus, a subcompartment of the nucleus organized around the rRNA-encoding region of the genome. This includes a large number of specific co-transcriptional and posttranscriptional modifications of rRNA nucleotides.

*To whom correspondence should be addressed. Tel: +49 69 7982 9525; Fax: +49 69 7982 9527; Email: entian@bio.uni-frankfurt.de

The most abundant rRNA modifications are 2′O-ribose methylations and pseudouridylations mediated by box C/D or H/ACA snoRNA-guided enzymes, respectively (7,8). In addition, some base modifications are introduced by specific and snoRNA-independent enzymes. In yeast, the N-dimethylation of two neighbouring adenosines at the 3′ end of 18S rRNA is catalyzed by Dim1 (9), and recently Bud23 was shown to catalyze the N7-methylation of guanosine 1575 (10). The unique hypermodification of U1191 in yeast 18S rRNA (U1248 of human 18S rRNA) to m1acp3Ψ (11) is located in the decoding domain of the ribosome and was recently suggested to be of importance for efficient 18S rRNA maturation and ribosome formation (12). The first step in introducing this hypermodification is the conversion from uridine to pseudouridine by the snR35 containing H/ACA-snoRNP (13). Thereafter, Ψ1191 becomes N1-methylated in the nucleolus, whereas the acp-modification is added in the cytoplasm (14). The methyl group as well as the acp-group are derived from *S*-adenosylmethionine (15,16), but the enzymes responsible for this hypermodification in eukaryotic cells are still unknown. For the archaeon *Haloferax volcanii* a 3-(3-amino-3-carboxypropyl)-uridine (acp3U) modification and for *Methanocaldococcus jannaschii* a nucleotide modification of unknown structure was shown to be present at the position homologous to yeast Ψ1191 (17).

An increasing number of rare autosomal-inherited human diseases have recently been attributed to mutations in proteins required for ribosome biogenesis and/or function (18). Many of these diseases show bone marrow defects, anaemia and severe developmental defects (19). The *SBDS* gene responsible for Shwachman–Bodian–Diamond syndrome (SBDS) encodes a homologue to the Sdo1 protein of *S. cerevisiae*, which is involved in the maturation of the 60S ribosomal subunit. SBDS patients show abnormal expression of ribosomal proteins, rRNA transcription- and rRNA-processing proteins (20). About 25% of the patients suffering from Diamond–Blackfan anaemia (DBA) carry mutations in the ribosomal protein Rps19 (21), which is important for the 3′ maturation of 18S rRNA in yeast and human cells (22–24).

We have recently shown that a specific point mutation within the Nep1 ribosome assembly protein, also referred to as Emg1 (25,26), causes Bowen–Conradi syndrome [BCS (MIM 211180)] (27). BCS results in severe pre- and postnatal growth and psychomotor retardation, microcephaly, micrognathia, rocker bottom feet and early childhood death (28). So far most BCS cases are found in high frequency in Hutterite families (1 in 355 births), but the recent identification of the BCS mutation is expected to result in an increasing number of identifiable cases outside the Hutterite population.

Nep1 is highly conserved in eukaryotes and the human Nep1 orthologue complements the function in a yeast *ScΔnep1* deletion (25,26). Nep1 is essential for 40S ribosomal subunit maturation (25,26) and our data suggested Nep1 to be involved in a methylation reaction (26). Recently, crystal structures of yeast Nep1 (*Sc*Nep1) (29) and its homologue from the archaeon *M. jannaschii* (*Mj*Nep1) (30) were solved. Both revealed folds typical for the SPOUT-family of methyltransferases (31). Members of the SPOUT family are known to introduce posttranscriptional *S*-adenosylmethionine-dependent RNA-methylations at 2′-OH-groups, at guanosine N1 or at the N3-atom of uridines or pseudouridines (32,33). The crystal structure of the *Mj*Nep1 dimer revealed a positively charged surface area poised for RNA-binding in a cleft at the dimer interface (30). Recently, we have shown that *Mj*Nep1 methylates Ψ-residues at the N1-position *in vitro* in a sequence-specific manner (34). The preference of *Mj*Nep1 for sequences resembling helix 35 in *M. jannaschii* 18S rRNA suggested that Nep1 might be responsible for a similar modification *in vivo*.

Here, we show for the first time that Nep1 specifically catalyzes the N1-methylation step during the biosynthesis of the unique hypermodified m1acp3Ψ at position Ψ1191 within loop 35 of eukaryotic 18S rRNA *in vivo*. Interestingly, the BCS mutation does not affect Ψ-methylation *per se*, but instead prevents the nucleolar localization of Nep1. Our data support a dual role of Nep1 as a methyltransferase and as a ribosome assembly factor and also provide reasons for the malfunction of the mutant protein in ribosome biogenesis and the BCS.

MATERIALS AND METHODS

Gene and protein nomenclature

The yeast *NEP1* gene is referred to as *ScNEP1*, the human *NEP1* gene as *HsNEP1* and the *M. jannaschii NEP1* gene as *MjNEP1*. The respective proteins are referred to as *Sc*Nep1, *Hs*Nep1 and *Mj*Nep1.

Plasmid constructions and yeast strains

Detailed descriptions are available in Supplementary Data.

Yeast media

Yeast strains were grown at 30°C (if not otherwise noted) in YEPD medium (1% yeast extract, 2% peptone, 2–4% glucose) or in synthetic dropout medium (0.5% ammonium sulphate, 0.17% yeast nitrogen base, 2–4% glucose). For selection on KanMX, G418 was added to the medium (0.2 mg/ml). For growth analysis of tc aptamer containing strains, cells were serially diluted and spotted on YEPD plates containing 0, 20 or 50 μM tetracycline. Growth was recorded after 3 days of incubation at 30°C in the dark. Diploid cells were sporulated on 1% potassium acetate plates for 3 days at 30°C.

Generation of stable human cell lines

Sequences coding for human *HsNep1* wild type or the D86G mutant were cloned into a pcDNA5/FRT/TO derivative for transfection of Flp-In T-REx-293T cells using the Flp-In T-REx system (Invitrogen). Stable 293T cell lines that express GFP fusions of human Nep1 wild type (*Hs*Nep1-GFP) or the $Nep1^{D86G}$ mutant ($Hs Nep1^{D86G}$-GFP) under control of the tetracycline-inducible promoter were generated according to the manufacturer's protocol.

^{14}C labelling of 18S rRNA nucleotide Ψ(U)1191

For specific isotope labelling of the 18S rRNA aminocarboxypropyl group yeast cells were grown with L-[1-^{14}C]-methionine. To enhance ^{14}C-labelling each utilized yeast strain carried a deletion of *MET13* (*ScΔmet13*), a gene encoding for the methylenetetrahydrofolate reductase involved in methionine biosynthesis (35). The *ScΔmet13* deleted strains were grown in synthetic medium with 20 μM methionine until OD_{600} of 2.5, harvested by centrifugation and adjusted to OD_{600} of 0.8 with methionine-free medium to which L-[1-^{14}C]-methionine (Hartmann Analytic, 0.1 mCi/ml, 54 mCi/mmol) was added rapidly to a final concentration of 18.5 μM with an activity of 1 μCi/ml. After incubation at 30°C for one generation time, cells were harvested by centrifugation.

Preparation of total rRNA

Total RNA from isotope labelled cells was isolated using the RNeasy Kit (QIAGEN) following the protocol for enzymatic cell lysis. Ribosomal RNAs were separated on a 4% denaturing polyacrylamide gel. For detection of specific 18S rRNA-labelling with L-[1-^{14}C]-methionine gels were stained with ethidium bromide, dried and analysed by autoradiography for 3–5 days using a storage phosphor screen. Signals were visualized with the Typhoon 9100 (GE Healthcare).

Separation and Isolation of 18S rRNA

rRNA was separated on a 4% acrylamide gel with 8 M urea. For the isolation of ^{14}C-labelled 18S rRNA, total RNA was separated and 18S rRNAs were eluted from gel slices with 2 M ammoniumacetate pH 5.3 (0.4 ml per 0.5 cm^2 gel, overnight incubation at 4°C). Eluted rRNA was precipitated with 2.5 vol 100 % ethanol and 1 vol 8 M lithium chloride, and finally dissolved in water.

For large-scale preparation of 18S rRNA, exponentially growing cells from 2 l YEPD medium were harvested and cell extracts were prepared using glass beads in a ribosome buffer without $MgCl_2$ (50 mM Tris–HCl pH 7.6, 50 mM NaCl, 1 mM DTT). Ribosome subunits were separated by gradient ultracentrifugation using 20–50% sucrose gradients in a SW28 rotor (Beckmann) for 21 h at 20 000 r.p.m. 40S subunits were collected with the Density Gradient Fractionation System (Teledyne Isco) and precipitated with 2 vol of 100% ethanol at 4°C for 16 h. Precipitated 40S subunits were dissolved in water and 18S rRNA was purified using the RNeasy Kit (QIAGEN) following the protocol for RNA cleanup. RNA was eluted in three subsequent steps with 35 μl water each.

High-performance liquid chromatography

18S rRNA was hydrolysed and dephosphorylated as previously described (36). Nucleosides from ^{14}C-labeling experiments were separated by RP-HPLC on an HXSil C18-Column (Hamilton, 250 × 4.6 mm, 5 μm) on an Agilent 1200 HPLC system. Buffer A (0.25 M ammonium acetate pH 6.0) and buffer B (40% acetonitrile) were used with the following HPLC conditions: flow rate 1.2 ml/min; 0% B for 2 min, to 50% B over 20 min, to 100% B over 5 min, held at 100% B for 3 min. Fractions of 15 s were collected and radioactivity was measured in a Wallac 1401 scintillation counter. Large-scale high-performance liquid chromatography (HPLC) experiments (100 pmol 18S rRNA) were performed using a Supelcosil LC-18-S column (Sigma; 250 × 4.6 mm, 5 μm) with a pre-column (4.6 × 20 mm) following the gradient conditions previously described (33). For mass spectrometry analysis nucleosides were collected from large-scale HPLC experiments and desalted twice over a Zorbax Eclipse XDB-C18 column (Agilent; 4.6 × 150 mm, 5 μm) using 5 mM ammonium acetate pH 6.0 with a flow rate of 0.5 ml/min. After buffer evaporation, samples were resolved in water and applied to ESI mass spectrometry on a MicroTof-QII (Bruker) in the negative ion mode. 5 mM TEAA buffer pH 7.0 with methanol (50%) was used as mobile phase.

Western blot analysis of 3xHA-Nep1

Protein extracts from HA-epitope tagged yeast strains were prepared using glass beads. Twenty micrograms total protein of each sample were separated with 12% sodium dodecyl sulphate (SDS) polyacrylamide gels and blotted on PVDF membranes (Millipore). Membranes were blocked with 5% non-fat dry milk and tagged proteins were detected with anti-HA monoclonal antibody (Roche; 1:1000 dilution) followed by anti-mouse IgG-conjugated horseradish peroxidase (BioRad; 1:10 000 dilution).

Protein localization

Yeast cells containing GFP-*Sc*Nep1 fusion encoding plasmids and a chromosomally integrated gene encoding for *Sc*Nop56-mRFP were grown to mid-logarithmic phase in synthetic medium lacking histidine. Protein localization was visualized using a Leica TCS SP5.

Expression of human *Hs*Nep1-GFP wild type or the *Hs*Nep1^{D86G}-GFP mutant fusion proteins under control of the tetracycline-inducible promoter in stable 293T cell lines was induced for 24 h by addition of 200 ng/ml doxycycline. Cells were fixed for 7 min in 3% (w/v) paraformaldehyde including 0.1% (w/v) glutardialdehyde, mounted in Vectashield containing DAPI and imaging was performed on a Leica TCS SP5.

Protein purification and gel filtration analysis

Wild-type yeast *Sc*Nep1 and the D90G mutant with an N-terminal 6xHis-tag were expressed from pQE-9 plasmids in *Escherichia coli* XL1-blue (Stratagene) and purified using HIS-Select Nickel Affinity Gel (Sigma).

Analytical gel filtrations were performed at room temperature on an ÄKTA FPLC system with a Superdex 75 100/300 column (GE Healthcare) equilibrated with 250 mM NaCl, 25 mM Tris/HCl, pH 7.5, 2 mM β-mercaptoethanol. Protein samples of 300 μl with different *Sc*Nep1 protein concentrations (1–216 μM) were prepared in the same buffer and equilibrated at 4°C for at least 12 h. The samples were loaded to the column using a 100-μl loop and separated at a flow rate of 0.5 ml/min. Absorbance was recorded at 280 nm. Molecular mass

standards were conalbumin (75 kDa), ovalbumin (43 kDa), carbonic anhydrase (29 kDa) and ribonuclease A (13.7 kDa) (GE Healthcare). The molecular masses of the standards were plotted versus log(M) to calculate the apparent Nep1 molecular weights. Thereafter, the apparent Nep1 molecular weights were plotted versus the respective Nep1 protein concentration. To determine the monomer/dimer dissociation constants, the following equation which describes a monomer/dimer equilibrium was fitted to this curve using the nonlinear least square algorithm of Origin 8 (OriginLab):

$$MW_{ap} = MW_M\left(2 - \left(\sqrt{K_{Dap}^2/16 + cK_{Dap}/2} - K_{Dap}/4\right)/c\right)$$

where MW_{ap} is the apparent molecular weight monomer, MW_M the molecular weight monomer, K_{Dap} the apparent monomer/dimer dissociation constant and c Nep1 the concentration applied to the column.

Fluorescence anisotropy measurements

For the fluorescence anisotropy measurements a 5′-fluorescein labelled RNA (5′-Fl-GACUCAACACG-3′) (Dharmacon) was used. Measurements were performed on a Fluorolog 3 spectrometer (Horiba Jobin Yvon) at 20°C in 2 ml polystyrene cuvettes. Excitation and emission wavelengths were set to 490 nm and 516 nm, respectively. *Sc*Nep1 protein was dialysed against 100 mM KCl, 25 mM Tris/HCl, 2 mM β-mercaptoethanol, pH 7.5 before the experiments and the same buffer was used during the anisotropy measurements. For *Sc*Nep1^{D90G} measurements, protein was added from concentrated stock solutions of at least 45 μM to a 20 nM solution of RNA while for *Sc*Nep1 wild-type measurements a 30 μM protein solution was adjusted to 20 nM RNA concentration and serially diluted with a 20 nM RNA solution. Plotted data points are means of at least three independent measurements. The binding curves were fitted to the equation

$$A = \frac{c}{c+K_D}A_I + A_F$$

where A is the fluorescence anisotropy, c Nep1 the monomer concentration, K_D the dissociation constant, A_I the increase of the fluorescence anisotropy due to formation of the RNA/Nep1 complex and A_F the fluorescence anisotropy of the free RNA, using the nonlinear least square algorithm of Origin 8 (OriginLab) to obtain the dissociation constants.

RNA methyltransferase activity assay

The RNA methylation activity was tested in a reaction mixture containing 50 mM KCl, 25 mM Tris/HCl, pH 7.5, 500 μM *S*-adenosylmethionine, 250 μM RNA (5′-GACΨCAACACG-3′) (Dharmacon) and 22 μM *Sc*Nep1. This mixture was incubated at 37°C for 30 min. For MALDI mass spectrometry samples from the RNA methylation reaction were diluted 1:10 with pure water. For mass analysis, 0.5 μl sample solution were mixed together with 2 μl matrix solution directly on the MALDI target and dried in a stream of air. 3-hydroxypicolinic acid (40 mg/ml in water) containing 5 mg/ml diammoniumhydrogencitrate was used as matrix. Mass spectra were recorded on a MALDI Orbitrap XL (Thermo Scientific) in positive ion mode. Resolution at this instrument was set to 30 000. Five to ten spectra were accumulated over a maximum of 80 laser shots, depending on the number of ions produced.

RESULTS

Identification of the Nep1 methyltransferase target site

The ribosome biogenesis cofactor Nep1 has been shown to possess a structure resembling that of members of the SPOUT methyltransferase family (29,30). The *S. cerevisiae* Nep1 RNA-binding motif which we identified (37) occurs at three positions within the 18S rRNA (nucleotides 349–354 near helix 12, 1190–1195 near helix 35 and 1566–1571 near helix 47 of yeast 18S rRNA). No base modifications are known adjacent to or within helix 12. Within the possible binding site of *Sc*Nep1 near helix 47, G1575 is methylated at N7. Recently, it was suggested that *Sc*Bud23 catalyses the G1575 N7-methylation (10). To exclude a potential role of *Sc*Nep1 in the m7G modification we performed aniline cleavage experiments (38; see also Supplementary Methods) with 18S rRNA from wild type and a *ScΔnep1 Δtma23* yeast strain, where the *ScΔtma23* deletion suppresses the lethal *ScΔnep1* phenotype (39). The 18S rRNA isolated from 40S subunits was cleaved by aniline at the 7-methylguanine residue at position 1575 resulting in a 3′-terminal 215-nt-long fragment in wild type. In the *ScΔnep1 Δtma23* strain the G1575 base methylation was unaffected because the corresponding aniline induced cleavage still occurred, indicating that *Sc*Nep1 is not responsible for this rRNA modification (Supplementary Figure S1).

As our *in vitro* experiments showed a specific pseudouridine N1-methyltransferase activity of *Mj*Nep1 if this Ψ is located at a position corresponding to Ψ1191 in the putative Nep1 binding site (34), we focused our attention to the region near helix 35 which contains the hypermodified nucleotide m1acp3Ψ at position 1191 (Figure 1A).

U1191 pseudouridylation requires the presence of the snoRNA snR35 and recently Liang *et al.* (12) reported a reduced translational rate, impaired ribosome function and a delay in 20S rRNA processing in *Δsnr35* deletants. Therefore, we tested for possible genetic interactions of a *Scnep1-1^{ts}* mutation with a *ScΔsnr35* deletion which prevents pseudouridylation. Indeed, a minor synthetic sick effect was observed for *Scnep1-1^{ts} Δsnr35* recombinants (Supplementary Figure S2) which provided evidence that pseudouridylation may support Nep1 function. In contrast to the recent report on a reduction in growth upon *ScΔsnr35* deletion in *S. cerevisiae* (12) no effects on growth became obvious, which shows that the fast-growing CEN.PK strains due to a different genetic background (40) do respond less sensitive to *Δsnr35* deletion as compared to the strains used in (12). Phenotypic differences upon gene deletions are often found between different yeast strains (40).

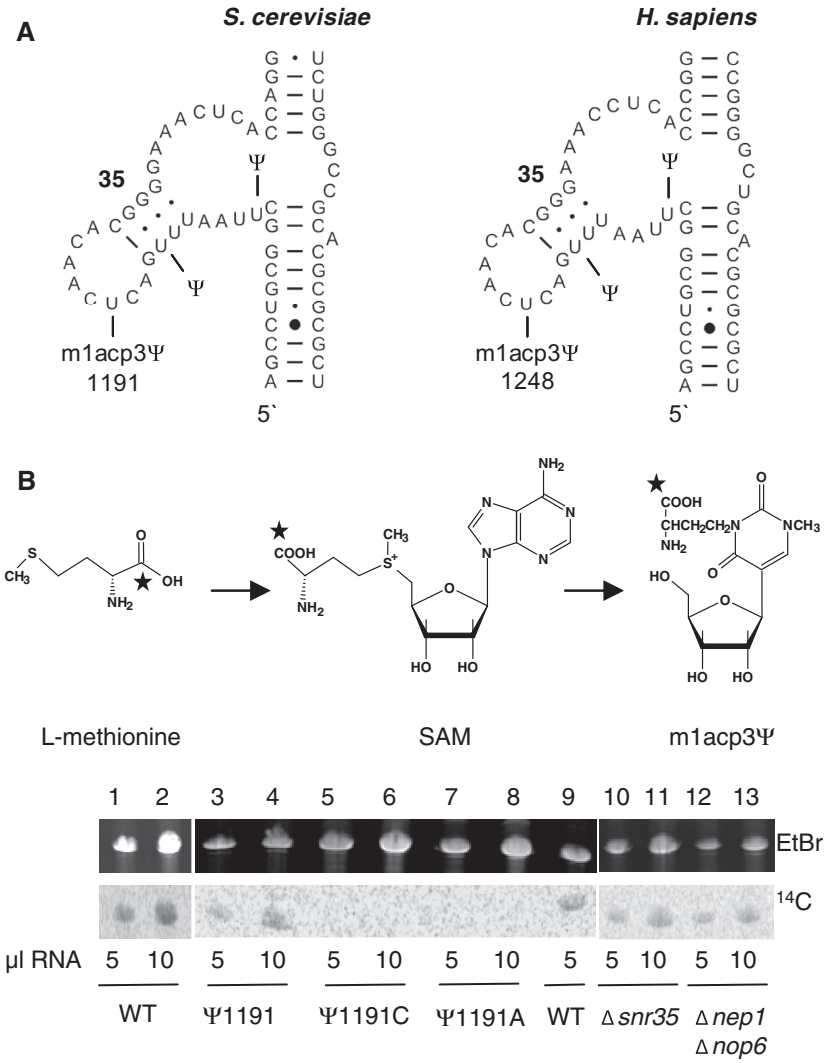

Figure 1. Analysis of the U1191 yeast 18S rRNA hypermodification. (**A**) The predicted secondary structure of a region of 18S rRNA (www.rna.ccbb.utexas.edu/) containing helix 35 and the hypermodified nucleotide m1acp3Ψ (1191 in *S. cerevisiae*, 1248 in *H. sapiens*) is shown. (**B**) Specific ^{14}C-aminocarboxypropyl-labeling of yeast 18S rRNA nucleotide U1191 with L-[1-^{14}C]-methionine. The asterisk indicates the ^{14}C-label (top). Total RNA was isolated from *ScΔmet13* cells after growth with L-[1-^{14}C]-methionine and separated by acrylamide gel electrophoresis (bottom). (Upper part) Ethidium bromide staining of RNA gels. (Lower part) Autoradiography of RNA gels. Samples of 5 and 10 µl total RNA from wild type (CEN.NM1-4D: WT, lanes 1, 2 and 9), rDNA deleted strains with plasmid encoded wild-type rDNA (CEN.BM146-1C: Ψ1191, lanes 3 and 4), plasmid encoded rDNA mutations U1191C (CEN.BM147-1C: Ψ1191C, lanes 5 and 6), U1191A (CEN.BM148-1C: Ψ1191A, lanes 7 and 8), a *ScΔsnr35* deleted strain (CEN.BM141-7G: *Δsnr35*, lanes 10 and 11) and a *ScΔnep1 Δnop6* deleted strain (CEN.BM140-11B: *Δnep1 Δnop6*, lanes 12 and 13) were loaded on the gel.

Helix 35 of 18S rRNA is strongly conserved in yeast and humans (Figure 1A) and is also present in the 16S rRNA of *M. jannaschii*. To investigate a possible function of Nep1 in Ψ1191 modification, we analysed the acp-modification in yeast 18S rRNA from wild-type cells and in a *ScΔnep1 Δnop6* strain, where the *ScΔnop6* deletion suppresses the lethal *ScΔnep1* phenotype (39). We specifically labelled the acp-group by cultivating wild-type and *ScΔnep1 Δnop6* cells with L-[1-^{14}C]-methionine because the C1- and C2-atoms of methionine are incorporated via *S*-adenosylmethionine into m1acp3Ψ 1191 (16). To enhance ^{14}C-labelling efficiency we used methionine auxotrophic yeast strains carrying a *ScΔmet13* deletion. Total RNA was isolated, separated by acrylamide gel electrophoresis and analysed for ^{14}C-labelling of the 18S rRNA by autoradiography. Strains with point mutations of U1191 to adenosine or cytosine served as controls for the specificity of the radioactive signal. Replacement of U1191 by any other base caused significant growth deficiencies. While strains with the wild-type rDNA plasmid had generation times of 2 h 30 min, U1191G replacement increased the generation times to 3 h 10 min, U1191A replacement to 3 h 40 min and U1191C replacement even to 5 h. The severe impact of U1191 replacement by any other base not only clearly shows the importance of U1191 for ribosome biogenesis and/or function, but also shows that a failure in Ψ1191 modification does not explain the essential phenotype of a *ScΔnep1* deletion.

Most remarkably, after gel electrophoresis of total RNA and a subsequent autoradiography no radiolabelling was observed for the A1191 and C1191 rRNA mutants (Figure 1B), whereas a weak but clear radioactive signal of 18S rRNA from the wild type was present. This clearly showed that the acp group of ^{14}C-methionine was specifically incorporated into 18S rRNA and also confirmed that Ψ1191 is the only base with an acp modification in the 18S rRNA. In case of the *ScΔnep1 Δnop6* double mutant, 18S rRNA was ^{14}C-labelled like wild type, demonstrating that Nep1 had no influence on the acp-modification of Ψ1191. Interestingly, the 18S rRNA of a *ScΔsnr35* mutant which prevents pseudouridylation at this position also contained the acp-modification, showing that the N3-position of U1191 can also be acp-modified (Figure 1B), which is in accordance with a strong stop in recent 18S rRNA primer extension studies with *ScΔsnr35* mutants (12).

The SPOUT methyltransferase Nep1 is required for Ψ1191 methylation

We then used the ^{14}C-acp label to identify the modified Ψ1191 nucleosides in yeast wild-type and *ScΔnep1* deletion strains. The 18S rRNAs from wild-type and *ScΔnep1Δnop6* mutants were hydrolysed and dephosphorylated, and the resulting nucleosides were separated by RP-HPLC. The ^{14}C-labelled nucleosides from wild type eluted 9.4 min after the elution gradient was started, whereas ^{14}C-labelled nucleosides from *ScΔnep1Δnop6* mutants had already eluted at 5.7 min (Figure 2A). An acp-labelled U1191 isolated from a *ScΔsnr35* snoRNA mutant that lacks pseudouridylation was eluted after 10.9 min (Figure 2A).

The altered elution time of the ^{14}C-acp-labelled nucleoside in the *ScΔnep1Δnop6* mutant suggested a change in the Ψ N1-modification pattern. To elucidate the chemical nature of the acp-modified nucleosides the 18S rRNAs from wild-type and mutant strains were purified in large scale, hydrolyzed and separated by RP-HPLC. The ratio of modified Ψ1191 nucleosides to the other major nucleosides (A, U, G, C) is ~1:400, which makes their isolation difficult. However, small peaks corresponding to the differently modified Ψ1191 in the RP-HPLC profile could be identified using the ^{14}C-label (Figure 2B).

In addition, the Ψ1191-modified nucleosides were analysed by electro spray ionization (ESI) mass spectrometry analysis. The molecular mass of the Ψ1191-modified nucleosides from wild type of 358.1215 Da [M-H] corresponded to the expected theoretical mass of m1acp3Ψ ($C_{14}H_{21}N_3O_8$ [M-H]: 358.1256 Da) (Supplementary Figure S3A). For the *ScΔnep1Δnop6* mutant the molecular mass of 344.1099 Da [M-H] was exactly as the theoretical mass of the non-methylated acp3Ψ nucleoside (Supplementary Figure S3B). Thus, the absence of Nep1 in a *ScΔnep1Δnop6* mutant results in the elimination of the methylation at position 1191, demonstrating that Nep1 is the methyltransferase responsible for the *in vivo* methylation of Ψ1191 in the 18S rRNA in yeast.

Functional analysis of the BCS yeast Nep1^{D90G} mutation

Our recent molecular analysis of the human BCS showed that this rare and severe disease is caused by a point mutation resulting in a D86G exchange in human Nep1 (27). To analyse the Nep1 malfunction in BCS, the BCS mutation was introduced into yeast Nep1 (*Sc*Nep1^{D90G}) and the resulting reading frame was placed under the recently described tetracycline aptamer regulatory system, where addition of tetracycline prevents translation of the corresponding mRNA (41). This allowed a gradual down-regulation of *Sc*Nep1 expression with increasing tetracycline concentrations. Without tetracycline no growth difference was observed for the *Sc*Nep1 wild type and the *Sc*Nep1^{D90G} BCS mutation. However, when the expression of *Sc*Nep1 and *Sc*Nep1^{D90G} was down-regulated, growth of the BCS mutant was significantly slowed down as compared to the wild type (Figure 3A). The expression levels of *Sc*Nep1 and *Sc*Nep1^{D90G} with and without tetracycline were very similar (Figure 3B). This clearly shows that the BCS mutation influences growth in yeast, consistent with the human condition.

The BCS protein loses its nucleolar localization

For further analysis, the cellular localization of the yeast (*Sc*Nep1^{D90G}) and human (*Hs*Nep1^{D86G}) BCS proteins was analysed using GFP-fusions. In yeast, the GFP-*Sc*Nep1^{D90G} fusion complemented growth in a *ScΔnep1* deletion after its multi-copy expression. Interestingly, the BCS *Sc*Nep1^{D90G} protein lost its exclusive nuclear localization. In GFP-*Sc*Nep1 wild-type cells a strong super-imposed signal was seen with Nop56-mRFP, which was used as a nucleolar marker, whereas for the GFP-*Sc*Nep1^{D90G} fusion the nuclear localization was strongly reduced and it showed distinct cytoplasmic staining (Figure 4A).

An even more pronounced effect was found for the human BCS *Hs*Nep1^{D86G} protein in stable human 293T cell lines that express GFP-fusions of human Nep1 wild type or the Nep1^{D86G} mutant. While wild-type *Hs*Nep1-GFP localized to the nucleus and showed strong nucleolar staining, the *Hs*Nep1^{D86G}-GFP mutant was nucleoplasmic but did not accumulate in the nucleolus and instead showed a weak cytoplasmic signal (Figure 4B). This is in accordance with our previous findings that the human D86G mutant protein showed a reduced nuclear level in BCS patient fibroblasts (27). Importantly, the BCS mutant loses its nucleolar localization, which could explain the malfunction in ribosome biogenesis and the BCS.

The BCS proteins show increased dimerization *in vitro*

Analysis of the human *Hs*Nep1^{D86G} protein showed a strongly increased interaction of the monomers in the yeast two-hybrid system (27). To biochemically confirm an enhanced BCS protein interaction yeast wild-type and yeast *Sc*Nep1^{D90G} proteins were expressed with an N-terminal hexahistidine tag (H_6) in *E. coli*, affinity purified and separated by gel filtration. Analytical gel

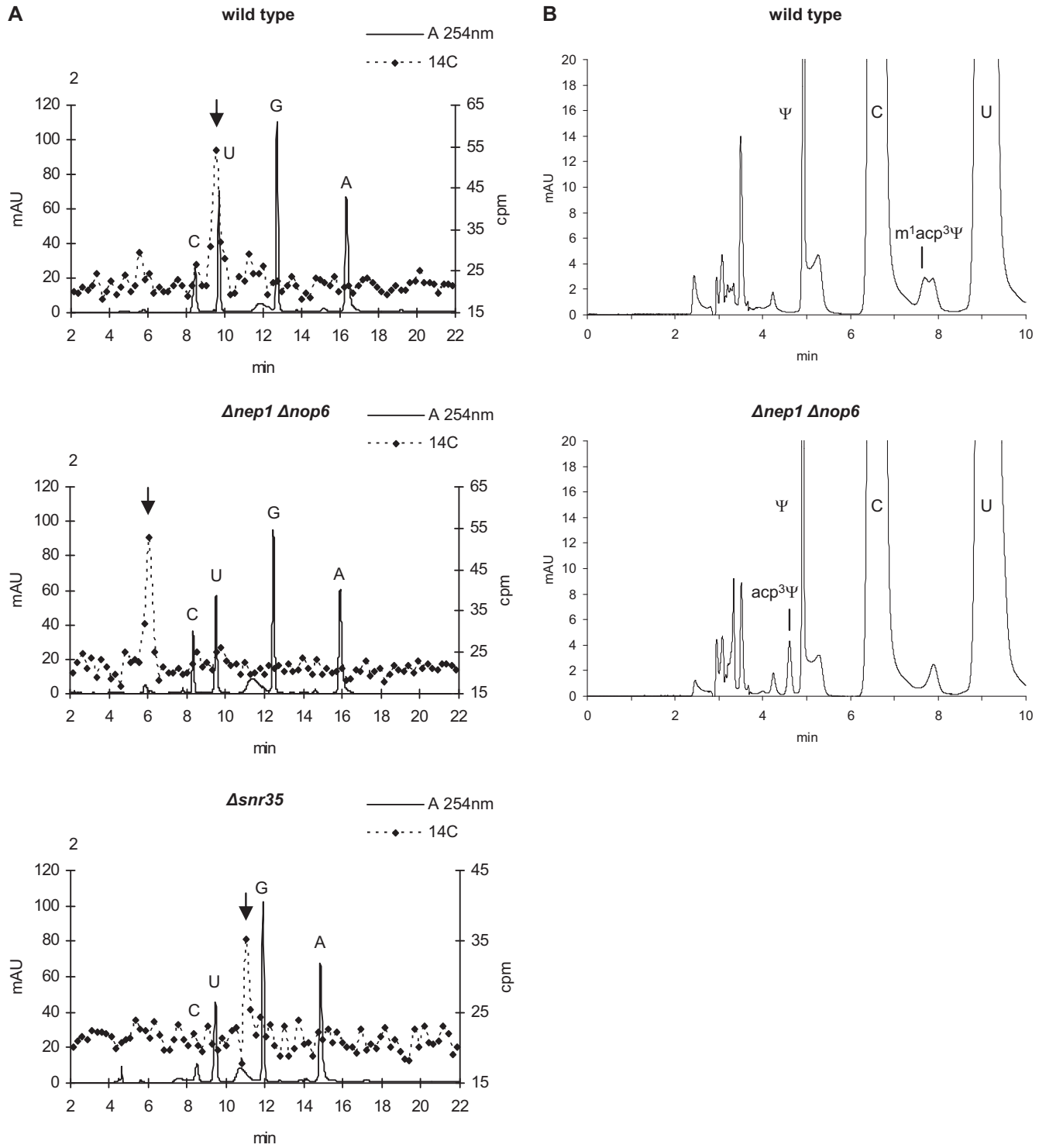

Figure 2. U1191 modifications in wild type, *ScΔsnr35* and *ScΔnep1 Δnop6* mutants. (**A**) RP-HPLC analysis of 18S rRNA nucleosides from *ScΔmet13* deleted acp-^{14}C-labelled cells. 18S rRNAs were isolated from denaturing polyacrylamide gels, hydrolysed and dephosphorylated to nucleosides, which were separated on an HXSil-C18 column. Fractions of 15 s each were collected and ^{14}C scintillation was counted. Dotted lines correspond to the scintillation profile, solid lanes correspond to the HPLC-spectrum detected at 254 nm. Peaks of standard nucleosides (C, U, G, A) are indicated. (**B**) Elution profiles of nucleosides from wild type (upper part) and a *ScΔnep1 Δnop6* mutant (lower part). 18S rRNAs were isolated from 40S ribosomal subunits, hydrolysed and dephosphorylated prior to RP-HPLC separation with a Supelcosil LC-18-S column.

filtrations over a wide range of different protein concentrations showed a concentration-dependent monomer/dimer equilibrium for the wild-type H_6-*Sc*Nep1 protein (Figure S4A). At low protein concentration (1 μM) wild-type H_6-*Sc*Nep1 was eluted at ~32 kDa, which is close to the molecular mass of the monomer (calculated molecular mass, 28.9 kDa), whereas at higher H_6-*Sc*Nep1 protein concentrations the equilibrium was shifted

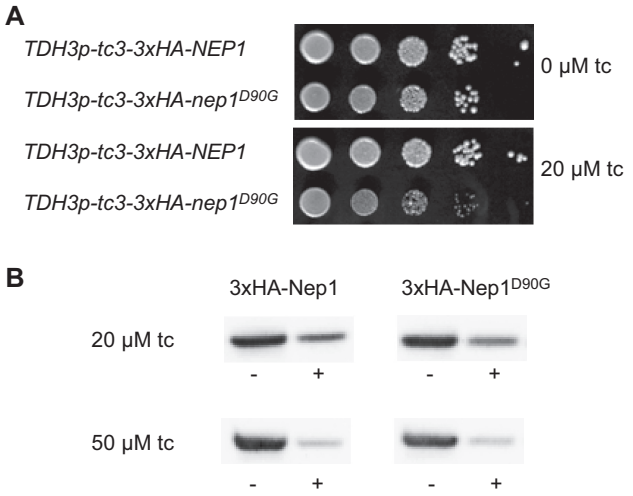

Figure 3. Functional analysis of the yeast Bowen–Conradi syndrome mutation. (**A**) *Sc*Nep1^{D90G} mutant growth defect after partial translational repression. Wild-type *ScNEP1* (CEN.PK935-2B) or *Scnep1*^{D90G} (CEN.BM113-4A) were expressed under control of the *ScTDH3*-promotor and three tc-aptamers. Serial dilutions were spotted on YEPD plates without or with 20 µM tetracycline. (**B**) Quantification of 3xHA-Nep1 and 3xHA-Nep1^{D90G} expression by western blot analysis. The 3xHA-Nep1 and 3xHA-Nep1^{D90G} levels were detected after 8 h growth without (–) or after addition of 20 or 50 µM tetracycline (+) to yeast strains CEN.PK935-2B (*TDH3p-tc-3xHA-NEP1*) and CEN.BM113-4A (*TDH3p-tc-3xHA-nep1*^{D90G}).

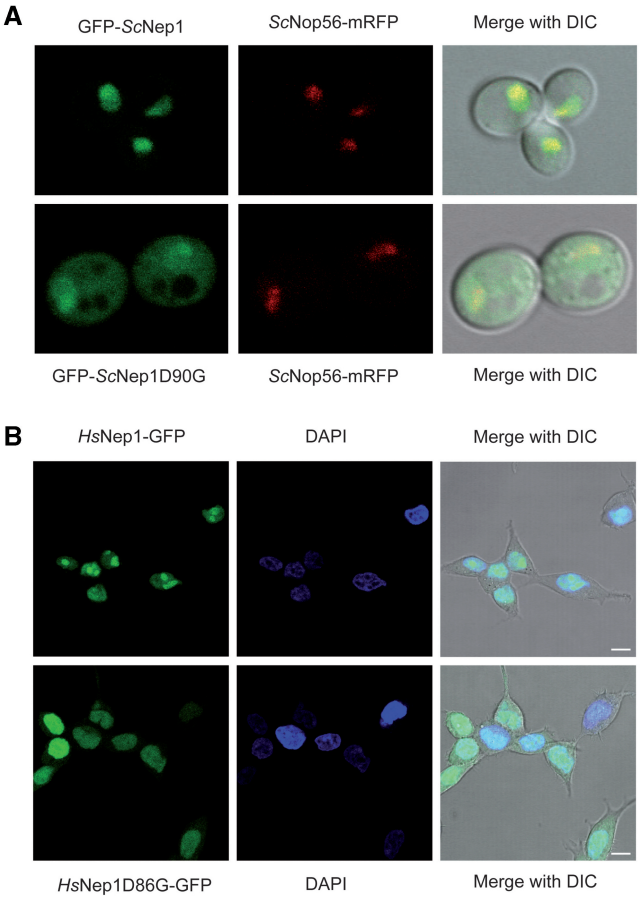

Figure 4. Intracellular localization of BCS-mutated Nep1 proteins. (**A**) Cellular localization of yeast wild-type *Sc*Nep1 (upper part) and the D90G mutant (lower part) using confocal microscopy. Both proteins were expressed as GFP-fusion together with the *Sc*Nop56-mRFP protein as a nucleolar marker. (Left) Green fluorescence (*Sc*Nep1); (middle) red fluorescence (*Sc*Nop56); (right) merge with differential interference contrast (DIC). (**B**) Intracellular localization of human *Hs*Nep1 (upper part) and the *Hs*Nep1^{D86G} mutant (lower part) after 24 h induction with 200 ng/ml doxycycline. The cellular localizations of the GFP-fusion proteins were analysed by confocal microscopy. (Left) Green fluorescence; (middle) DAPI staining; (right) merge with differential interference contrast (DIC). Scale bar: 10 µm.

towards the dimeric form (48 kDa at protein concentration of 216 µM, calculated molecular mass: 57.8 kDa). By contrast, comparable gel filtrations with the H$_6$-Nep1^{D90G} protein (Figure S4B) always provided higher molecular weights as compared to the H$_6$-*Sc*Nep1 wild-type protein. The strong difference between the H$_6$-*Sc*Nep1 and the H$_6$-*Sc*Nep1^{D90G} mutant protein became even more obvious when the molecular weights were plotted against the protein concentrations (Figure 5A). These data clearly show that the *Sc*Nep1^{D90G} mutation caused strongly enhanced dimerization as compared to the wild-type *Sc*Nep1 protein. Based on the equation for monomer/dimer equilibria the data were fitted to the curve to calculate apparent monomer/dimer dissociation constants (see 'Materials and Methods' section). The *Sc*Nep1^{D90G} mutant apparent K_D (5.8 ± 3.2 µM) was more than 23-fold lower as compared to the *Sc*Nep1 wild-type apparent K_D (134.5 ± 17 µM), which explains the strongly enhanced dimerization of the *Sc*Nep1^{D90G} mutant protein. The apparent molecular weights for the wild-type monomer (MW_{ap} = 31.1 kDa) and the mutant monomer (MW_{ap} = 30.7 kDa) derived from this fittings were remarkably close to the expected molecular weight of the monomer (MW = 28.9 kDa) and confirm the accuracy of the measurements.

The BCS proteins have increased RNA affinity *in vitro*

As only the Nep1 dimer can efficiently bind to the target RNA, we assumed that the *Sc*Nep1^{D90G} mutant protein might have an increased RNA-binding affinity. Therefore, we determined the RNA/Nep1 dissociation constants by fluorescence anisotropy measurements using 5′-fluorescein labelled RNA (5′-Fl-GACUCAACACG-3′) (Figure 5B). Indeed the dissociation constant of *Sc*Nep1^{D90G} (K_D = 0.36 ± 0.04 µM) was 17-fold decreased as compared to that of wild-type *Sc*Nep1 (K_D = 6.29 ± 0.98 µM). This shows a strongly increased RNA-binding affinity of the BCS-mutated Nep1 protein.

Ψ1191 methylation activity of the yeast BCS^{D90G} mutated Nep1

Our finding that the BCS yeast *Sc*Nep1 mutation increases dimerization motivated us to analyse the methylation activity of the BCS-mutated enzyme. According to our recently developed Nep1 *in vitro* methylation assay (34), we used an RNA oligonucleotide equivalent to nucleotides 1188–1198 of yeast 18S rRNA as substrate (5′-GACΨCA

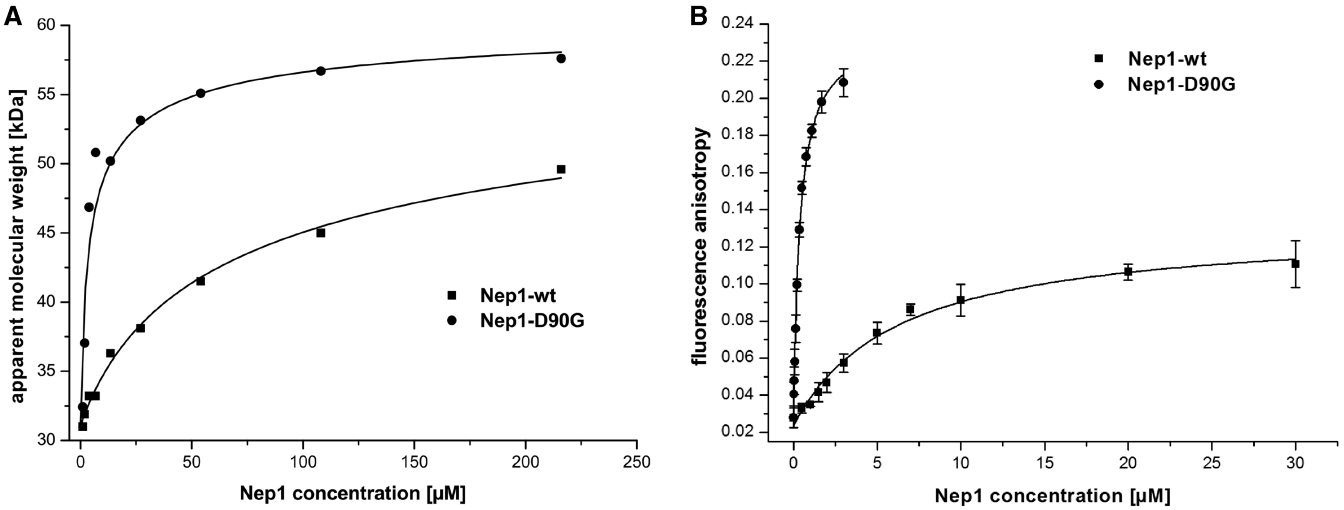

Figure 5. Dimerization and RNA-binding affinity of BCS-mutated yeast *Sc*Nep1^{D90G}. (**A**) Apparent molecular weights of *Sc*Nep1 (squares) and *Sc*Nep1^{D90G} (circles) calculated from retention volumes after gel filtrations at nine different protein concentrations (1–216 μM) are plotted versus the *Sc*Nep1 concentration to calculate the apparent monomer/dimer dissociation constants. Dissociation constants derived from the fits were 134.5 (±17) μM for wild-type *Sc*Nep1 and 5.8 (±3.2) μM for *Sc*Nep1^{D90G}. The calculated apparent molecular weights of the monomers were 31.1 (±0.4) kDa for wild-type *Sc*Nep1 and 30.7 (±1.4) kDa for *Sc*Nep1^{D90G}. (**B**) *Sc*Nep1 binding to a 5′-fluorescein labelled RNA (5′-Fl-GACUCAACACG-3′) determined by fluorescence anisotropy. Shown are mean and standard deviation of three measurements. The binding curves were fitted to a one site binding model with one binding site per monomer. Dissociation constants derived from the fit are 6.29 (±0.98) μM for wild-type *Sc*Nep1 and 0.38 (±0.04) μM for *Sc*Nep1^{D90G}.

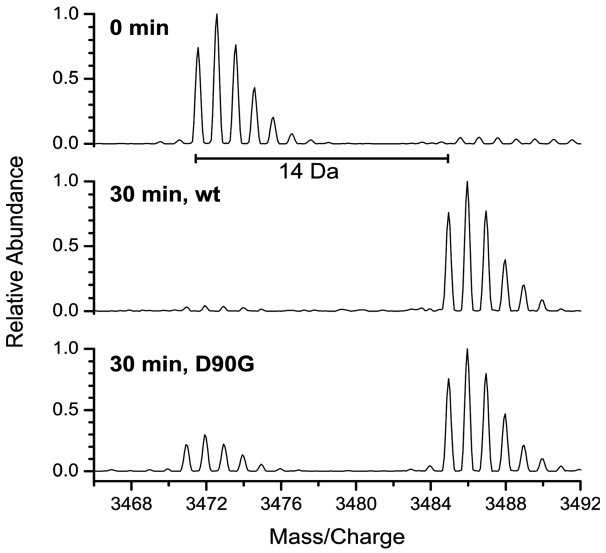

Figure 6. RNA-methylation activity of wild type and BCS-mutated *Sc*Nep1. Analysis of *in vitro* RNA-methylation with yeast *Sc*Nep1 and BCS-mutated *Sc*Nep1^{D90G}. MALDI mass spectra of an RNA oligonucleotide (5′-GACΨCAACACG-3′) containing a pseudouridine in the position corresponding to nucleotide 1191. The mass of the RNA oligonucleotide (upper part) increases by 14 Da 30 min after addition of *S*-adenosylmethionine (*Sc*Nep1, middle part, *Sc*Nep1^{D90G}-mutated protein, lower part).

ACACG-3′) and analyzed the reaction products by MALDI-mass spectrometry. Thereby we could show that the yeast BCS protein methylated the target RNA as efficiently as the *Sc*Nep1 wild-type protein *in vitro* (Figure 6). These data suggest that Nep1, in addition to rRNA methylation, has a second role in ribosome biogenesis.

S-adenosylmethionine suppression of *nep1-1^{ts}* is independent of Ψ1191 methylation

A dual Nep1 function was also strongly supported by results from recombination experiments of the *ScΔsnr35* mutation with the previously described *Scnep1-1^{ts}* mutation which grows at elevated temperature if suppressed by an external *S*-adenosylmethionine supply (26). External *S*-adenosylmethionine suppressed the *ScΔsnr35 nep1-1^{ts}* strain, although this strain cannot methylate U1191 due to the *ScΔsnr35* deletion (Figure 7). Thus, substrate (*S*-adenosylmethionine) binding restores *Sc*Nep1-1^{ts} function even if it is not required as a substrate for RNA methylation.

DISCUSSION

Ribosome biogenesis is one of the most complex biosynthetic pathways in eukaryotic cells. It is highly regulated and in addition to the 79 core proteins of the ribosome, ~180 proteins and 75 snoRNAs are required for ribosome synthesis (4–6). The additional proteins and snoRNAs fulfil two major functions, either rRNA processing and modification or ribosome assembly. Although the specific molecular function of most rRNA modifications is still not resolved, many of these modifications are highly conserved in eukaryotic rRNAs, which clearly shows their physiological importance. A unique modification is the uracil hypermodification in yeast (U1191) and human (U1248) 18S rRNA (11), which is similar to modifications found in some archaea (17). U1191 is located in loop 35 of the yeast 18S rRNA in the decoding region of the ribosome and has been shown to be important for ribosome function (12). The rRNA sequence of loop 35 in yeast is strongly conserved in the human 18S rRNA

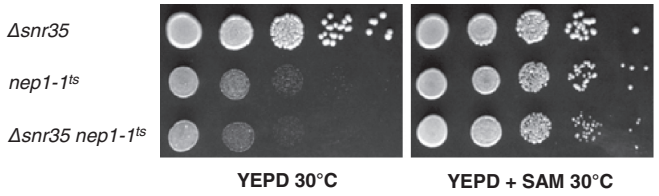

Figure 7. *S*-adenosylmethionine suppression of the *Scnep1-1*^{ts} mutant incubated at 30°C. Yeast strains CEN.PK1016-9C (*ScΔsnr35*), CEN.PK1016-4C (*Scnep1-1*^{ts}) and CEN.PK1016-7A (*Scnep1-1*^{ts} *Δsnr35*) were spotted on YEPD medium without (left) or with *S*-adenosylmethionine (0.2 mg/ml, right).

(see also Figure 1A) which also supports its significance for ribosome function. The hypermodification of U1191 involves three modification steps: First, a pseudouridylation supported by snoRNA snR35 in yeast or snoRNA ACA13 in humans; second, N1-methylation; and, third, N3-acp modification, resulting in 1-methyl-3-(3-amino-3-carboxypropyl)-pseudouracil. Whereas the acp-modification takes place in the cytoplasm, the N1-methylation occurs during ribosome biogenesis in the nucleus.

Here, we show that the SPOUT methyltransferase Nep1 (Emg1) catalyses the N1-Ψ1191 methylation *in vivo*. Interestingly, our results with *ScΔsnr35* deletion mutants show that the methylation is specific for Ψ, whereas the cytoplasmic acp-modification also occurs at the N3 position of uracil which is in accordance with recent findings (12). Furthermore, a reduced translation rate and impaired ribosome function were also reported for *ScΔsnr35* deletion mutants (12). The fact that the remaining U1191 is still acp-modified possibly indicates that missing N1-methylation might cause these effects.

The functional importance of U1191 in the 18S rRNA is further supported by our finding that replacement of U1191 by any other base had a strong impact on yeast growth. While replacement with G and A caused significant growth retardation, C1191 replacement mutants were hardly viable. This could be due to either structural effects or the fact that these mutations interfere with Nep1 binding. Nevertheless, the G/C/A1191 mutations were viable, which shows that the absence of an N1-methylation at Ψ1191 does not explain the lethal phenotype of a *ScΔnep1* mutation. This clearly shows that Nep1 Ψ1191 methylation is not the only function of Nep1. This also became obvious in the *Sc*Nep1-1^{ts} experiments with *S*-adenosylmethionine. Even after *ScΔsnr35* deletion when no U1191 pseudouridylation and, as shown here and previously (12), no N1-methylation occurs, the addition of *S*-adenosylmethionine restores growth of a *Scnep1-1*^{ts} mutant at elevated temperatures. Our results clearly show a dual function of Nep1 as a methyltransferase and as an assembly protein in ribosome biogenesis. This is also in accordance with the recent observation that *Sc*Nep1 mutations which prevent *S*-adenosylmethionine binding can still provide the essential Nep1 function (29). Similar findings have also been reported for *Sc*Dim1 which catalyses the N-dimethylation of A1781 and A1782 at the 3′ end of the 18S rRNA (9) and also for *Sc*Bud23, recently shown to catalyse the N7-methylation of G1575 (10). Interestingly, all three RNA modifications are dispensable for cell viability although *Sc*Nep1, *Sc*Dim1 and *Sc*Bud23 are essential for growth and ribosome biogenesis.

The dual function of Nep1 is also of major importance for the human BCS, where a specific missense mutation causes a severe disorganization of ribosome biogenesis (27). Therefore, unravelling the physiological function of the Nep1 protein in ribosome biogenesis is of key importance to understand the molecular basis for this severe developmental disease and to possibly develop strategies to compensate for its malfunction. Fortunately, Nep1 is a highly conserved eukaryotic protein and the human Nep1 protein is functional in yeast (26), which allows the use of yeast as a model system to study Nep1 function in ribosome biogenesis.

Although the corresponding yeast BCS protein (*Sc*Nep1^{D90G} protein) still methylated its target RNA almost as efficiently as the *Sc*Nep1 wild-type protein, the D90G mutant was less viable. In yeast and human Nep1 the BCS mutation causes several severe changes in the physical properties of the protein. Importantly, these are increased dimerization and decreased protein stability (data not shown) which in consequence results in strongly diminished levels of Nep1 in the nucleolus. This is in accordance with several experimental data: the reduced amount of Nep1^{D86G} in the nuclei of patient fibroblasts as compared to healthy fibroblasts (27), the strongly diminished amount of *Sc*Nep1^{D90G} in the yeast nucleus, and the fact that stable human cell lines do not accumulate *Hs*Nep1^{D86G} in the nucleolus. Possibly, increased dimerization might reduce BCS-mutated Nep1 import into the nucleus in yeast (and less severely also in human cells), abolish its nucleolar accumulation in human cells (and less severely in yeast) and/or disturb Nep1 interaction with co-factors, thereby preventing its function as a ribosome assembly protein. These findings further support a dual function of Nep1 in ribosome biogenesis. While the BCS mutation does not interfere with RNA methylation *in vitro*, the observed malfunction may directly interfere with ribosome biogenesis. Affinity capture studies showed that *Sc*Nep1 forms a macromolecular complex with several ribosome assembly proteins (e.g. *Sc*Nop14, *Sc*Nop1, *Sc*Noc4, *Sc*Utp30 and *Sc*Krr1) (42,43). Additionally, we have previously observed that multi-copy expression of *Sc*Rps19, a protein of the small ribosome subunit, suppresses the *Scnep1-1*^{ts} phenotype more efficiently as compared to the *ScΔnep1* deletion, indicating that Nep1 supports Rps19 entry into the pre-ribosomal complex (37).

In summary, we show for the first time that yeast Nep1 catalyses the *in vivo* N1-methylation of the unique hypermodified Ψ1191 within the decoding region of the ribosome and that the mutation causing the BCS has no effect on the catalytic function of Nep1. Instead, it leads to severe changes in the physical properties of Nep1, which most likely prevent its accumulation in the nucleolus and its subsequent function as a ribosome assembly protein.

SUPPLEMENTARY DATA

Supplementary Data are available at NAR Online.

ACKNOWLEDGEMENTS

The authors are grateful to Barbara Triggs-Raine for helpful discussion, suggestions, and critical reading of the manuscript and Heinz Schewe for his excellent support in confocal laser microscopy. MTB and MSL would like to thank Enrico Schleiff for support.

FUNDING

The SFB579 'RNA-Ligand interactions', project B3; the Cluster of Excellence Frankfurt: Macromolecular Complexes; the Center of Biomolecular Magnetic Resonance (BMRZ); Aventis Foundation through an endowed professorship for chemical biology (to J.W.). Funding for open access charge: the Cluster of Excellence Frankfurt: Macromolecular Complexes.

Conflict of interest statement. None declared.

REFERENCES

1. Bernstein,K.A., Gallagher,J.E., Mitchell,B.M., Granneman,S. and Baserga,S.J. (2004) The small-subunit processome is a ribosome assembly intermediate. *Eukaryot. Cell*, **3**, 1619–1626.
2. Grandi,P., Rybin,V., Bassler,J., Petfalski,E., Strauss,D., Marzioch,M., Schafer,T., Kuster,B., Tschochner,H., Tollervey,D. *et al*. (2002) 90S pre-ribosomes include the 35S pre-rRNA, the U3 snoRNP, and 40S subunit processing factors but predominantly lack 60S synthesis factors. *Mol. Cell*, **10**, 105–115.
3. Warner,J.R. (1999) The economics of ribosome biosynthesis in yeast. *Trends Biochem. Sci.*, **24**, 437–440.
4. Fromont-Racine,M., Senger,B., Saveanu,C. and Fasiolo,F. (2003) Ribosome assembly in eukaryotes. *Gene*, **313**, 17–42.
5. Tschochner,H. and Hurt,E. (2003) Pre-ribosomes on the road from the nucleolus to the cytoplasm. *Trends Cell Biol.*, **13**, 255–263.
6. Venema,J. and Tollervey,D. (1999) Ribosome synthesis in *Saccharomyces cerevisiae*. *Annu. Rev. Genet.*, **33**, 261–311.
7. Kiss-Laszlo,Z., Henry,Y., Bachellerie,J.P., Caizergues-Ferrer,M. and Kiss,T. (1996) Site-specific ribose methylation of preribosomal RNA: a novel function for small nucleolar RNAs. *Cell*, **85**, 1077–1088.
8. Ganot,P., Bortolin,M.L. and Kiss,T. (1997) Site-specific pseudouridine formation in preribosomal RNA is guided by small nucleolar RNAs. *Cell*, **89**, 799–809.
9. Lafontaine,D., Delcour,J., Glasser,A.L., Desgres,J. and Vandenhaute,J. (1994) The *DIM1* gene responsible for the conserved m6(2)Am6(2)A dimethylation in the 3′-terminal loop of 18 S rRNA is essential in yeast. *J. Mol. Biol.*, **241**, 492–497.
10. White,J., Li,Z., Sardana,R., Bujnicki,J.M., Marcotte,E.M. and Johnson,A.W. (2008) Bud23 methylates G1575 of 18S rRNA and is required for efficient nuclear export of pre-40S subunits. *Mol. Cell. Biol.*, **28**, 3151–3161.
11. Maden,B.E., Forbes,J., de Jonge,P. and Klootwijk,J. (1975) Presence of a hypermodified nucleotide in HeLa cell 18 S and *Saccharomyces carlsbergensis* 17 S ribosomal RNAs. *FEBS Lett.*, **59**, 60–63.
12. Liang,X.H., Liu,Q. and Fournier,M.J. (2009) Loss of rRNA modifications in the decoding center of the ribosome impairs translation and strongly delays pre-rRNA processing. *RNA*, **15**, 1716–1728.
13. Samarsky,D.A., Balakin,A.G. and Fournier,M.J. (1995) Characterization of three new snRNAs from *Saccharomyces cerevisiae*: snR34, snR35 and snR36. *Nucleic Acids Res.*, **23**, 2548–2554.
14. Brand,R.C., Klootwijk,J., Planta,R.J. and Maden,B.E. (1978) Biosynthesis of a hypermodified nucleotide in *Saccharomyces carlsbergensis* 17S and HeLa-cell 18S ribosomal ribonucleic acid. *Biochem. J.*, **169**, 71–77.
15. Enger,M.D. and Saponara,A.G. (1968) Incorporation of 14C from [2-14C]methionine into 18 S but not 28 S RNA of Chinese hamster cells. *J. Mol. Biol.*, **33**, 319–322.
16. Saponara,A.G. and Enger,M.D. (1974) The isolation from ribonucleic acid of substituted uridines containing alpha-aminobutyrate moieties derived from methionine. *Biochim. Biophys. Acta*, **349**, 61–77.
17. Kowalak,J.A., Bruenger,E., Crain,P.F. and McCloskey,J.A. (2000) Identities and phylogenetic comparisons of posttranscriptional modifications in 16 S ribosomal RNA from *Haloferax volcanii*. *J. Biol. Chem.*, **275**, 24484–24489.
18. Scheper,G.C., van der Knaap,M.S. and Proud,C.G. (2007) Translation matters: protein synthesis defects in inherited disease. *Nat. Rev. Genet.*, **8**, 711–723.
19. Ganapathi,K.A. and Shimamura,A. (2008) Ribosomal dysfunction and inherited marrow failure. *Br. J. Haematol.*, **141**, 376–387.
20. Rujkijyanont,P., Adams,S.L., Beyene,J. and Dror,Y. (2009) Bone marrow cells from patients with Shwachman–Diamond syndrome abnormally express genes involved in ribosome biogenesis and RNA processing. *Br. J. Haematol.*, **145**, 806–815.
21. Draptchinskaia,N., Gustavsson,P., Andersson,B., Pettersson,M., Willig,T.N., Dianzani,I., Ball,S., Tchernia,G., Klar,J., Matsson,H. *et al*. (1999) The gene encoding ribosomal protein S19 is mutated in Diamond–Blackfan anaemia. *Nat. Genet.*, **21**, 169–175.
22. Leger-Silvestre,I., Caffrey,J.M., Dawaliby,R., Alvarez-Arias,D.A., Gas,N., Bertolone,S.J., Gleizes,P.E. and Ellis,S.R. (2005) Specific role for yeast homologs of the Diamond–Blackfan anemia-associated Rps19 protein in ribosome synthesis. *J. Biol. Chem.*, **280**, 38177–38185.
23. Choesmel,V., Bacqueville,D., Rouquette,J., Noaillac-Depeyre,J., Fribourg,S., Cretien,A., Leblanc,T., Tchernia,G., Da Costa,L. and Gleizes,P.E. (2007) Impaired ribosome biogenesis in Diamond–Blackfan anemia. *Blood*, **109**, 1275–1283.
24. Idol,R.A., Robledo,S., Du,H.Y., Crimmins,D.L., Wilson,D.B., Ladenson,J.H., Bessler,M. and Mason,P.J. (2007) Cells depleted for *RPS19*, a protein associated with Diamond Blackfan anemia, show defects in 18S ribosomal RNA synthesis and small ribosomal subunit production. *Blood Cells Mol. Dis.*, **39**, 35–43.
25. Liu,P.C. and Thiele,D.J. (2001) Novel stress-responsive genes *EMG1* and *NOP14* encode conserved, interacting proteins required for 40S ribosome biogenesis. *Mol. Biol. Cell*, **12**, 3644–3657.
26. Eschrich,D., Buchhaupt,M., Kötter,P. and Entian,K.D. (2002) Nep1p (Emg1p), a novel protein conserved in eukaryotes and archaea, is involved in ribosome biogenesis. *Curr. Genet.*, **40**, 326–338.
27. Armistead,J., Khatkar,S., Meyer,B., Mark,B.L., Patel,N., Coghlan,G., Lamont,R.E., Liu,S., Wiechert,J., Cattini,P.A. *et al*. (2009) Mutation of a gene essential for ribosome biogenesis, *EMG1*, causes Bowen–Conradi syndrome. *Am. J. Hum. Genet.*, **84**, 728–739.
28. Lowry,R.B., Innes,A.M., Bernier,F.P., McLeod,D.R., Greenberg,C.R., Chudley,A.E., Chodirker,B., Marles,S.L., Crumley,M.J., Loredo-Osti,J.C. *et al*. (2003) Bowen–Conradi syndrome: a clinical and genetic study. *Am. J. Med. Genet. A*, **120A**, 423–428.
29. Leulliot,N., Bohnsack,M.T., Graille,M., Tollervey,D. and Van Tilbeurgh,H. (2008) The yeast ribosome synthesis factor Emg1 is a novel member of the superfamily of alpha/beta knot fold methyltransferases. *Nucleic Acids Res.*, **36**, 629–639.
30. Taylor,A.B., Meyer,B., Leal,B.Z., Kotter,P., Schirf,V., Demeler,B., Hart,P.J., Entian,K.D. and Wohnert,J. (2008) The crystal structure of Nep1 reveals an extended SPOUT-class methyltransferase fold and a pre-organized SAM-binding site. *Nucleic Acids Res.*, **36**, 1542–1554.
31. Anantharaman,V., Koonin,E.V. and Aravind,L. (2002) SPOUT: a class of methyltransferases that includes spoU and trmD RNA methylase superfamilies, and novel superfamilies of predicted

prokaryotic RNA methylases. *J. Mol. Microbiol. Biotechnol.*, **4**, 71–75.
32. Tkaczuk,K.L., Dunin-Horkawicz,S., Purta,E. and Bujnicki,J.M. (2007) Structural and evolutionary bioinformatics of the SPOUT superfamily of methyltransferases. *BMC Bioinformatics*, **8**, 73.
33. Ero,R., Peil,L., Liiv,A. and Remme,J. (2008) Identification of pseudouridine methyltransferase in *Escherichia coli*. *RNA*, **14**, 2223–2233.
34. Wurm,J.P., Meyer,B., Bahr,U., Held,M., Frolow,O., Kotter,P., Engels,J.W., Heckel,A., Karas,M., Entian,K.D. *et al.* (2010) The ribosome assembly factor Nep1 responsible for Bowen–Conradi syndrome is a pseudouridine-N1-specific methyltransferase. *Nucleic Acids Res.*, **38**, 2387–2398.
35. Raymond,R.K., Kastanos,E.K. and Appling,D.R. (1999) *Saccharomyces cerevisiae* expresses two genes encoding isozymes of methylenetetrahydrofolate reductase. *Arch. Biochem. Biophys.*, **372**, 300–308.
36. Gehrke,C.W. and Kuo,K.C. (1989) Ribonucleoside analysis by reversed-phase high-performance liquid chromatography. *J. Chromatogr.*, **471**, 3–36.
37. Buchhaupt,M., Meyer,B., Kötter,P. and Entian,K.D. (2006) Genetic evidence for 18S rRNA binding and an Rps19p assembly function of yeast nucleolar protein Nep1p. *Mol. Genet. Genomics*, **276**, 273–284.
38. Zueva,V.S., Mankin,A.S., Bogdanov,A.A. and Baratova,L.A. (1985) Specific fragmentation of tRNA and rRNA at a 7-methylguanine residue in the presence of methylated carrier RNA. *Eur. J. Biochem.*, **146**, 679–687.
39. Buchhaupt,M., Kötter,P. and Entian,K.D. (2007) Mutations in the nucleolar proteins Tma23 and Nop6 suppress the malfunction of the Nep1 protein. *FEMS Yeast Res.*, **7**, 771–781.
40. Entian,K.-D. and Kötter,P. (2007) In Stansfield,I. and Stark,M.J.R. (eds), *Methods in Microbiology*, Vol. 36. Academic Press Ltd., San Diego, pp. 629–666.
41. Kötter,P., Weigand,J.E., Meyer,B., Entian,K.D. and Suess,B. (2009) A fast and efficient translational control system for conditional expression of yeast genes. *Nucleic Acids Res.*, **37**, e120.
42. Gavin,A.C., Bosche,M., Krause,R., Grandi,P., Marzioch,M., Bauer,A., Schultz,J., Rick,J.M., Michon,A.M., Cruciat,C.M. *et al.* (2002) Functional organization of the yeast proteome by systematic analysis of protein complexes. *Nature*, **415**, 141–147.
43. Collins,S.R., Kemmeren,P., Zhao,X.C., Greenblatt,J.F., Spencer,F., Holstege,F.C., Weissman,J.S. and Krogan,N.J. (2007) Toward a comprehensive atlas of the physical interactome of *Saccharomyces cerevisiae*. *Mol. Cell Proteomics*, **6**, 439–450.